International Journal of Non–Linear Mechanics 163 (2024) 104751

Contents lists available at ScienceDirect

International Journal of Non-Linear Mechanics

journal homepage: www.elsevier.com/locate/nlm

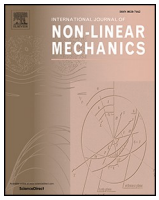

Non-linear tendon fatigue life under uncertainties

Mariana Rodriguez Reinoso [a,b], Paola Antonaci [a,b], Nicola M. Pugno [c,d], Cecilia Surace [a,b,*]

[a] Laboratory of Bioinspired Nanomechanics, Politecnico di Torino, Italy
[b] Department of Structural, Geotechnical and Building Engineering, Politecnico di Torino, Italy
[c] Laboratory for Bioinspired, Bionic, Nano, Meta, Materials & Mechanics, Department of Civil, Environmental and Mechanical Engineering, University of Trento, Via Mesiano 77, 38123 Trento, Italy
[d] School of Engineering and Materials Science, Queen Mary University of London, Mile End Road, E1 4NS, London, United Kingdom

ARTICLE INFO

Keywords:
Tendon fatigue life
Generalised Paris Erdogan equation
Monte Carlo analysis
Self healing

ABSTRACT

Tendons play a pivotal role in facilitating joint movement by transmitting muscular forces to bones. The intricate hierarchical structure and diverse material composition of tendons contribute to their non-linear mechanical response. However, comprehensively grasping their mechanical properties poses a challenge due to inherent variability in biological tissues. This necessitates a thorough examination of uncertainties associated with properties measurements, particularly under diverse loading conditions. Given the cyclic loading experienced by tendons throughout an individual's lifespan, understanding their mechanical behaviour under such circumstances becomes crucial.

This study addresses this need by introducing a generalised Paris Erdogan Law tailored for non-linear materials. To examine uncertainties within this proposed framework, Monte Carlo Analysis is employed. This approach allows for a thorough exploration of the uncertainties associated with tendon mechanics, contributing to a more robust comprehension of their behaviour under cyclic loading conditions.

Finally, self-healing has been integrated into the fatigue law of tendons through the proposal of a healing function, formulated as a polynomial function of the maximum stress. This approach allows to account for an increase in the number of cycles for each stress value due to self-repair after the damage event generated by long-term cycling load over the individual's life span.

1. Introduction

Tendons are connective tissues that play a crucial role on joint movements, since they enable to transfer the forces developed by muscles to the bones thus allowing locomotion [1]. Due to their high tensile strength, tendons efficiently transmit bursting forces much like springs, while also providing the flexibility necessary for a wide range of joint motions. Their structure allows to perform this role in such an efficient way, that they have a damping effect during the initial part of muscles force transmission and during high impact loading, while allowing at the same time an instantaneous strain transfer during movements [2,3]. In other words, tendon compliance is able to decrease the cost of muscular contraction by reducing the contractile velocity and length change for a given movement while boosting the power output of muscle-tendon units [4].

Tendons normally are subject to high levels of in vivo stresses [5]; they undergo small repetitive strains that cause microinjuries that gradually accumulate [6,7]. As a result, tendons are prone to present some overuse injuries which are collectively referred to as tendinopathy. The latter is related to a poor healing response, with tenocyte degeneration and random proliferation, collagen fibre disruption, and an increase in non-collagenous matrix [8,9]. In literature different studies have shown that low levels of post operative active forces applied to the repair site in the immediate postoperative period improve the tendon healing efficiency, and the application of excessive stress to an immature repair site would lead to a gap formation and poor clinical results [10,11].

For a comprehensive understanding of the mechanism of tendon overuse and therefore their fatigue damage progression towards tendinopathy or rupture, several authors have performed experimental analysis on animal tendons due to their wide availability, considering in vivo and ex vivo experimental methods [12]. Among the ex vivo experimental tests, Wang et al. [13] and Ker et al. [14] analysed cycling loading of Wallaby tail tendons, Pedaprolu et al. analysed rat Achilles

* Corresponding author. Laboratory of bioinspired Nanomechanics, Politecnico di Torino, Italy.
E-mail address: cecilia.surace@polito.it (C. Surace).

https://doi.org/10.1016/j.ijnonlinmec.2024.104751
Received 5 January 2024; Received in revised form 5 April 2024; Accepted 23 April 2024
Available online 7 May 2024

tendons [15], Fung et al. analysed rat flexor digitorum longus [16], other studies such as Soslowsky et al. [17] and Scott et al. [18] analysed rats supraspinatus tendons. Among the in vivo experimental test, Fung et al. [19] and Andarawis et al. [20] analysed rat patellar tendons under cycling loading, Sereysky et al. [21] analysed murine patellar tendons. Experimental data on fatigue tests in human soft tissues are extremely important to improve the knowledge in this field, however only few authors report human tendon data in the current scientific literature. Schetchman et al. report the fatigue behaviour of 90 specimens of Human Extensor Digitorum Longus (EDL) tendons evaluating nine different stress levels [22], Wren et al. report the fatigue behaviour under cycling loading for 25 specimens for human Achilles tendon [23]. Firminger et al. report the fatigue behaviour of 30 specimens of Human patellar tendon [24].

Soft tissues typically present non-linear mechanical response. More precisely, the mechanical behaviour of tendons is viscoelastic, thus, their load-displacement relationships are rate-dependent and history-dependent. A typical viscoelastic J-shaped stress-strain curve for tendon shows three different regions: a toe region for low stress due to tendon compliance (the stretch increases significantly as the load increases), a linear region at greater stresses and strains where the tendon stiffness increases up to reaching a fairly uniform elastic modulus, and finally a failure zone [16,19,25–27]. Typically, the linear region is predominant with respect to the others, indeed during a hysteresis loop, the tendon returns up to 90–95% of the stored energy and dissipate about 5–10% [4]. In addition, the mechanical behaviour of soft tissues normally presents a high degree of variability, due to internal and external factors. Indeed, the results of ex-vivo tests may vary according to the specimen, the location of harvesting, the conservation method, the experimental setup and measuring of the specimens. Therefore, even if an accurate mechanical model can be formulated, the model may not necessarily be adequate to predict the behaviour of another specimen. Since it is impossible to achieve a full knowledge of the all the parameters of the mechanical model, some assumptions are needed, and this introduces uncertainties into the results.

Over the time, few authors have developed fibrous soft tissues fatigue models with the aim to predict the number of cycles for fatigue failure [28–31]. In particular, Bosia et al. developed a model for fatigue of self-healing soft nanomaterial as tendons [30], Adeeb et al. applied the notions of Linear Fracture Mechanics for the development of fatigue behaviour of tendon models [31]. In both studies, the authors considered the Paris law for fatigue damage propagation as the starting point for their models: due to its robustness and suitability for multiple applications to different materials, the authors convey that this fatigue damage propagation law should be appropriate also for tendons and ligaments. However, the use of the Paris Law to describe the crack propagation in a non-linear material might be a restrictive approach that does not capture the innate non-linear mechanical behaviour of tendons.

In this context, it may be difficult to give an accurate prediction of the level of damage within a biological structure, because of the random variations and extremely high variability in terms of geometry and other mechanical features of the specimens. This suggests that also their lifetime will be a random variable likewise. Given the uncertain nature of the parameters, it might be useful to obtain boundaries for the estimation of the lifetime of the structure under study.

The analysis of uncertainties on the constitutive modelling for soft tissues is still in early stage. A recent study developed by Hosseini Nasab et al. analysed the accuracy of the estimation of the contact force due to the uncertainties in the parameters related to the muscle-tendon system by a probabilistic approach [32]. A study by Balzani et al. proposed a computational method for the assessment of rupture probabilities in soft collagenous tissues [33]. Another study of Haughton et al. proposed a new microstructural hyperelastic model for the mechanical behaviour of tendons, and to account for the parameters uncertainties they employed the Markov chain Monte Carlo algorithm [34]. In this context, Montecarlo Method can be employed to investigate the propagation of uncertainty on the lifetime prediction, and it appears to be one of the most suitable methods for modelling complex systems with multiple variables and uncertainties [34–36].

The main objectives of this paper are: (i) the development of a Generalised Paris-Erdogan (GPE) law for non-linear materials, and (ii) the analysis of the uncertainties that encompass the tendon fatigue mechanical behaviour by using Monte Carlo (MC) method. The GPE law here proposed will be developed considering some of the principles used by Carpinteri et al. for the fracture behaviour of Functionally Graded Materials (FGMs) [37], in which the stress intensity factor, rather than being a constant, varies with the structural size, the nominal strength and the fracture toughness of the material. Other principles employed by Pugno et al. regarding Atomistic Fracture [38] will also be included. The parameters for the proposed GPE will be obtained by integration within a genetic algorithm that performs data fitting between experimental data and the number of cycles obtained by integration for each stress value. In this study an experimental dataset for EDL tendons will be considered [22].

Furthermore, following a similar approach for the introduction of self-healing effect by Bosia et al. [29] an additional analysis will be performed considering the introduction of the healing rate within the GPE approach here proposed. The healing effect will be considered as a function of other parameters rather than a constant, as suggested in Ref. [29]. In particular, it will be introduced as a function of the maximum stress applied on the tendon, assuming that, for a given healing rate value η, it increases up to a critical stress value. Subsequently, the healing rate value starts to decrease due to the formation of the gap.

The paper is structured as follows: in section 2 the development of the GPE law is explained; in Section 3 the numerical approach for GPE integration is presented; In section 4 the method for the introduction of the Healing Function (HF) is shown; In section 5 the Monte Carlo analysis is described; in section 6 the results are shown and discussed.

2. Development of the Generalised Paris Erdogan law for non-linear materials

2.1. Linear elastic fracture mechanics principles and fatigue life

According to Linear Elastic Fracture Mechanics principles, for a rectangular plate of finite dimensions, with a mode I crack subjected to uniaxial tension, the stress intensity factor (SIF) denoted as K_I regulates the amplification of the applied stress σ in the field near to the crack tip. The SIF is expressed as shown in equation (1), where: Y is a function that depends on the crack and loading geometries; 2a represents the crack's width. In the case of a finite plate with a central crack, the value of the function Y is reported in equation (2), where 2b denotes the plate's width.

$$K_I = Y\sigma\sqrt{\pi a} \tag{1}$$

$$Y = \sqrt{sec\left(\frac{\pi a}{2b}\right)} \tag{2}$$

The critical energy release rate J_C, is a mechanical property that describes the ability of a material to resist the propagation of cracks. It is normally determined by making an initial notch, or crack, in the material and measuring the energy required to create a determined amount of new crack area [39,40]. According to Linear Elastic Fracture Mechanics, for the case of an isotropic linear elastic material there is a relationship between the failure stress σ_f and the half crack length a, as reported in Equation (3) (where E is the Elastic Modulus of the material and Y is a function of the crack and loading geometries). The parameter $(J_C E)^{1/2}$ is known as the Critical Stress Intensity Factor K_{IC}.

$$K_{IC} = \sqrt{J_c E} = Y\sigma_f\sqrt{\pi a} \tag{3}$$

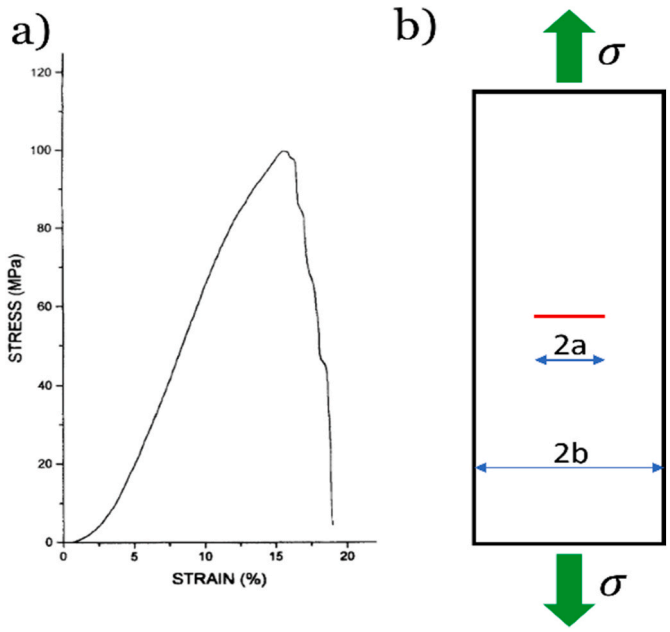

Fig. 1. (a) A Typical Stress- Strain Curve for EDL tendons from Schechtman et al. [22], (b) Tendon modelled as a slender rectangular plate, subjected to uniaxial tension, with a Type 1 crack located in the centre of the plate.

The Paris-Erdogan law is an empirical model that describes the progressive growth of a crack under cycling loading conditions in linear elastic materials. It expresses a power relationship between the rate of the crack growth with respect to the number of cycles, $da/\,dN$, and the difference $\Delta\sigma$ between the maximum and the minimum stress levels applied during the cyclic loading: $\Delta\sigma = \sigma_{max} - \sigma_{min}$. It is shown in equation (4), where C and m_p are the Paris constants, that can be determined experimentally [30].

$$\frac{da}{dN} = C\left(Y\Delta\sigma\sqrt{\pi a}\right)^{m_p} = C(\Delta K_I)^{m_p} \tag{4}$$

2.2. Generalised Paris -Erdogan law for non-linear materials

Tendons exhibit non-linear mechanical behaviour, as already mentioned in Section 1. Fig. 1a illustrates a typical stress-strain curve for Human Extensor Digitorum Longus (EDL) tendons, reproduced from the work of Schechtman et al. [22]. The curve displays a typical viscoelastic J-shaped profile, characterised by three distinct regions: a toe region for low stress; a linear region at higher stresses and strains, where the tendon stiffness increases to achieve a fairly uniform elastic modulus; and finally, a failure zone.

In this context, the traditional Paris-Erdogan law may not be the most suitable model to describe the crack growth under cyclic loading, due to material non-linearity. Therefore, in the following a generalised Paris-Erdogan law is proposed for non-linear materials. The tendon specimen under consideration can be modelled as a slender rectangular plate of finite dimensions, subjected to uniaxial tension. As in the previous section, it is hypothesised that the specific damage being examined involves a central fatigue crack exhibiting mode I opening, with the crack length extending perpendicularly to the loading axis. The crack's width is represented by 2a, while the plate's width is denoted by 2b, as shown in Fig. 1b.

According to [38], equation 1 can be generalised for non-linear elastic materials, as shown in Equation 5, where the stress-strain constitutive law is expressed as $\sigma \propto \varepsilon^k$. Here k is a constant, and if $k > 1$ it implies hyper-elasticity, if $k < 1$ it implies elasto-plasticity, while if $k = 1$ it implies linear elasticity [38]. Equation 6 delineates the range of the stress intensity factor. The parameter α represents the power stress-singularity, modified from the classical value of 1/2, being $\alpha = k/(k+1)$ [41].

$$K_{NL} = Y\sigma(\pi a)^{\alpha} b^{\left(\frac{1}{2}-\alpha\right)} \tag{5}$$

$$\Delta K_{NL} = Y\Delta\sigma(\pi a)^{\alpha} b^{\left(\frac{1}{2}-\alpha\right)} \tag{6}$$

Introducing equation (6) in equation (4) the following equation is obtained:

$$\frac{da}{dN} = C\left(Y\Delta\sigma(\pi a)^{\alpha} b^{\left(\frac{1}{2}-\alpha\right)}\right)^{m_p} \tag{7}$$

Defining the generalised stress intensity factor $K^*_{NL} = Y\sigma(\pi a)^{\alpha}$ and the generalised SIF range $\Delta K^*_{NL} = Y\Delta\sigma(\pi a)^{\alpha}$, equation (8) is obtained.

$$\frac{da}{dN} = C\left(\Delta K^*_{NL} b^{\left(\frac{1}{2}-\alpha\right)}\right)^{m_p} \tag{8}$$

Designating $C^*_{NL} = C\left(b^{\left(\frac{1}{2}-\alpha\right)}\right)^{m_p}$ equation (4) can be written as:

$$\frac{da}{dN} = C^*_{NL}\left(\Delta K^*_{NL}\right)^{m_p} \tag{9}$$

According to the work of Carpinteri and Pugno [37] it is possible to define a generalised critical stress intensity factor as follows, where UTS is the ultimate tensile strength:

$$K^*_{IC} = (1-\alpha)UTS\left(\frac{2K_{IC}}{UTS}\right)^{2\alpha} \tag{10}$$

During cyclic loading, the crack length will consistently increase. The criterion for terminating the process is determined by reaching the point at which the tendon specimen fails, marked by the generalised SIF reaching the critical generalised SIF K^*_{IC} . This threshold can be considered a critical value beyond which the material succumbs to fracture.

3. Numerical approach for GPE integration

3.1. Experimental data collection

The experimental data were collected from a study of Schechtman et al. in which the authors analysed the fatigue behaviour of ninety specimens of Human Extensor Digitorum Longus (EDL) tendons under square cycling loading with minimum stress level almost equal to zero and a maximum stress level in the range 10%–90% of the Ultimate Tensile Strength UTS (100 MPa), and a frequency loading (1, 2, 3, 4 Hz) that changed according to the stress level that was applied [22].

3.2. Integration of the generalised Paris- Erdogan law for non-linear materials

In this section, the GPE law for non-linear materials (equation (9)) is integrated employing a forward Euler method. In particular, the GPE law has been considered written in its inverse form as shown in equation (11). The integration requires determining the most suitable values for the material constants K_{IC}, C and m_p, which play a crucial role on the description of the material behaviour during cycling loading, and therefore the rate of the crack growth with respect to the number of cycles. A Genetic Algorithm (GA) is employed to perform the optimisation of this constants within the MATLAB environment, allowing to find the values $m_{bestfit}$, $C_{bestfit}$ and $K_{IC\ bestfit}$. The objective function f chosen to minimise with the GA algorithm is a sum of two terms. The first term $E1$ represents the sum of the relative error with respect to the number of cycles obtained by fitting N_{fit}, while the second term $E2$ pertains to the sum of the relative errors with respect to the

Table 1
Values for the upper and lower research boundaries with their respective units in square brackets.

Variable	min	max
m_p	4	6
C $[\mathbf{MPa}^{-m_p}\ \mathbf{m}^{m_p/2+1}]$	10^{-7}	10^{-5}
K_{IC} $[\mathbf{MPa}\sqrt{\mathbf{m}}]$	3	6

experimental number of cycles, N_{exp}.

$$\frac{dN}{da} = \left(C^*_{NL}\left(\Delta K^*_{NL}\right)^{m_p}\right)^{-1} \tag{11}$$

$$E1 = \sum abs\left(\frac{N_{exp} - N_{fit}}{N_{fit}}\right) \tag{12}$$

$$E2 = \sum abs\left(\frac{N_{exp} - N_{fit}}{N_{exp}}\right) \tag{13}$$

$$f = E1 + E2 \tag{14}$$

The parameters set for the integration were as follows: the initial half-crack width $a_0 = b/6$, with $b = 1.5$ mm representing the tendon's half-width; the ultimate tensile strength $UTS = 100$ MPa. The power of the stress singularity α was determined based on the work by Bosia et al., where $k = 2.33$, resulting in $\alpha = 0.7$ [30]. The values chosen for the search space are outlined in Table 1. The boundaries for the critical SIF K_{IC} were selected to encompass values found in the literature for other biological tissues [40]. Meanwhile, the values for the dimensionless constant m_p in the Paris-Erdogan law were set based on the various values obtained in the work of Adeeb et al. for EDL tendons [31]. Regarding parameter C, due to a lack of available literature data on its specific value for biological soft tissues, its boundaries have been determined after conducting some preliminary GA parameter optimisations. These boundaries encompass the entire range of values obtained during the optimisation process.

4. Introduction of the healing rate

Self-healing and remodelling processes occur within in vivo tissues, enabling them to heal microtraumas caused by repetitive or more extreme activities and stresses such as normal walking or sporting. However, all literature on the fatigue life of human tendons has been obtained using in vitro experimental tests, resulting in an underestimation of in vivo tendon fatigue life [30]. Drawing from ex vivo tendon mechanical properties and incorporating the self-healing effect, this section proposes a fatigue life model that may accurately estimate tendon fatigue life in vivo. A previous work of Bosia et al. introduced the concept of self-healing effect on the damage equation for tendons by considering the healing rate η. Healing effect is a function of time and damage level. The authors hypothesised that being the loading slow enough, the effect of time can be neglected and therefore only the dependence on the damage level is significant. As a first approximation, the authors assumed that η is a constant and that the term of the initial crack size a_i can be modified to $a_i\,(1-\eta)$. The healing rate value η can assume values from 0 to 1, being $\eta = 0$ the case in which there is no self-healing effect [30].

To the authors' best knowledge, self-healing is strongly dependent on the load that the tendon undergoes [30]. Several authors affirm that low levels of post operative active forces applied to the repair site in the immediate postoperative period improve the tendon healing efficiency, and the application of excessive stress to an immature repair site would lead to a gap formation and poor clinical results [10,11]. On the light of this, in this study the self-healing effect will be considered within the GPE approach with $\alpha = 0.7$, by modifying the expression of the crack size a to $a(1 - HF)$ where HF is the Healing Function. The HF will be considered as dependent on the stress level applied and the healing rate η; its value increases until a threshold stress value called critical stress σ_c, and for stress values higher that σ_c the value of HF starts decreasing.

According to the literature, following tendon injury, early mobilisation during the initial post-operative period accelerates the healing process. Specifically, low loads applied during passive rehabilitation protocols facilitate tissue remodelling. However, active rehabilitation protocols involving higher loads have been shown to yield the best results in terms of mechanical properties and collagen turnover [9,42–44].

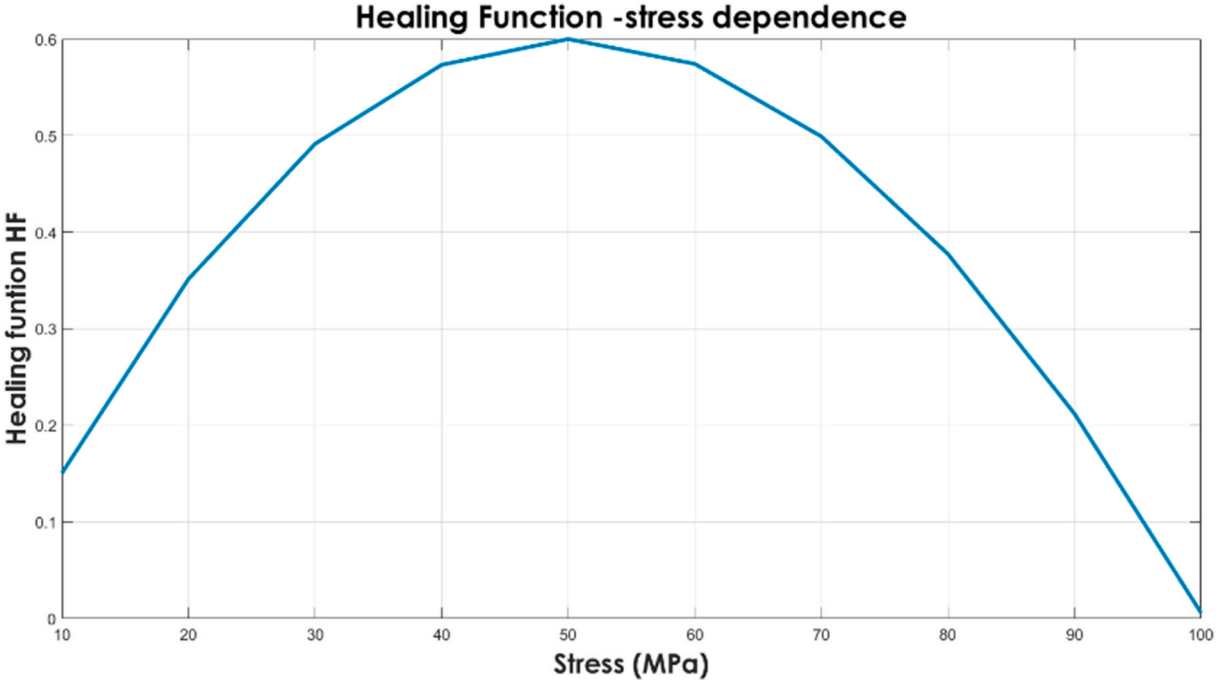

Fig. 2. Healing function for $\eta = 0.6$.

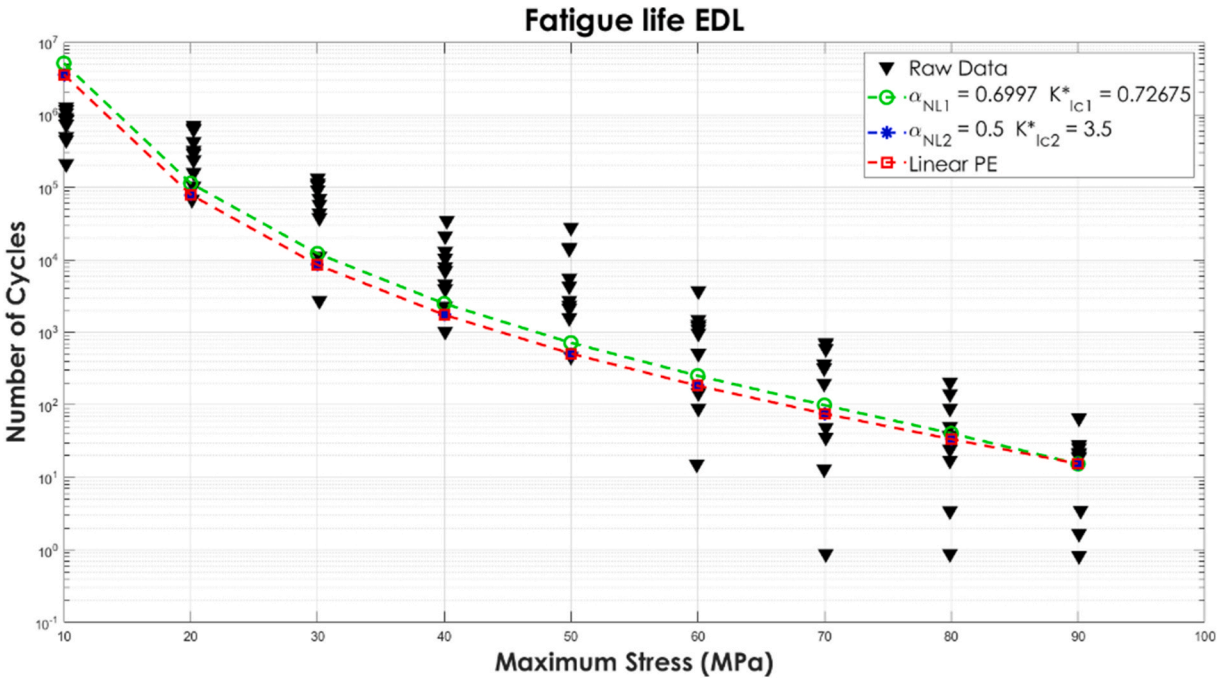

Fig. 3. Fatigue life of EDL tendons considering GPE and traditional PE law, for the value of $\alpha = 0.5$ the GPE and the linear PE lines are superimposed, where the units of K^*_{IC} are $[MPa\, m^{\alpha}]$.

Nevertheless, this enhancement of the healing effect persists only until a certain critical stress is reached, beyond which the healing effect of the tendon diminishes due to the formation of a gap between the tendon stumps [45]. Although the critical stress σ_c is not known, in this paper it has been assumed to reach the value of 0.5 times the ultimate tensile strength (UTS) to encompass the range of stresses developed during active motion. This is based on the observation that the stresses present in the Achilles Tendon during running activities are approximately 55 MPa, with the UTS being around 110 MPa [46,47].

Therefore, it has been hypothesised that the *HF* exhibits a polynomial trend over the course of the tendon life cycles. The chosen polynomial equation is reported in equation (15), where x is the difference between the experimental maximum stress at each level and the critical stress $\sigma_{exp} - \sigma_c$ divided by the value of the critical stress that in this study was set as $\sigma_c = 0.5\, UTS$ (see equation (16)). Meanwhile the value of the healing rate η may vary within the range $[0 - 0.6]$ as reported by Bosia et al. [30]. Fig. 2 reports the graph for the Healing function. For the introduction of the HF, equation (11) was considered: here, the expression of the generalised stress intensity factor K^*_{NL} was modified to the healing generalised stress intensity factor $\widehat{K^*_{NL}}$, and specifically the expression of half crack size a was replaced by $a(1 - HF)$ as shown in equation (17).

$$HF = 0.1\eta x^3 - 1.1\eta x^2 + \eta \tag{15}$$

$$x = \frac{\sigma_{exp} - \sigma_c}{\sigma_c} \tag{16}$$

$$\widehat{K^*_{NL}} = Y\sigma(\pi a(1 - HF))^{\alpha} \tag{17}$$

5. Monte Carlo analysis

When addressing the evaluation of mechanical properties in biological materials, several challenges arise due to the considerable variability among samples. This variability stems from factors such as differences in the site of harvesting, variations between animal models, and diverse experimental setups, protocols, and animal handling practices. The types of variability encountered in animal models can be categorised into three groups: (i) variability introduced by the experimenter, (ii) inherent variability of the specimens, and (iii) induced variabilities (i.e. variations resulting from the interaction between inherent differences among samples or individuals and external factors associated with experimental protocols or sample handling) [42]. Consequently, working with biological tissues inherently involves uncertainties and parameter variability [43]. In light of these challenges, Monte Carlo (MC) analysis proves invaluable, as it allows to take into account uncertainties by using probabilistic distributions to represent variables and parameters, enabling the prediction of realistic outcomes. This method effectively accommodates both small and large uncertainties and captures partial correlations among different variables and parameters [44].

MC analysis stands out as one of the most widely employed methods for analysing uncertainties across various fields. It finds application in scenarios characterised by a certain degree of uncertainty, such as determining the elastic properties in carbon fibre composites [45], identifying viscoelastic properties through elastography [46], and assessing the impact of alterations in moment arms and muscle-tendon properties on the accuracy of predictions in muscle function models [47].

To comprehensively integrate the proposed GPE law and MC analysis, this section also explores the GPE equation in its inverse form. The numerical integration employed a forward Euler explicit recursion method implemented within the MATLAB environment. The experimental data used in this study are derived from EDL tendons [22], where the authors measured the number of cycles for each of the 90 samples under investigation, with 10 samples for each applied stress level. Given the absence of specific guidance on probability distributions for GPE approach parameters, an initial consideration of a uniform distribution was made. Subsequently, for comparison purposes, a normal distribution was adopted.

In both cases, the mean values for parameters m_p and C were set to the values obtained from the GA, i.e., $m_{best\ fit}$ and $C_{best\ fit}$. The MC simulation assumes statistical independence of the parameters.

A number of 10,000 sample runs of the integration were conducted in order to obtain an accuracy in the range of two decimal places, as the

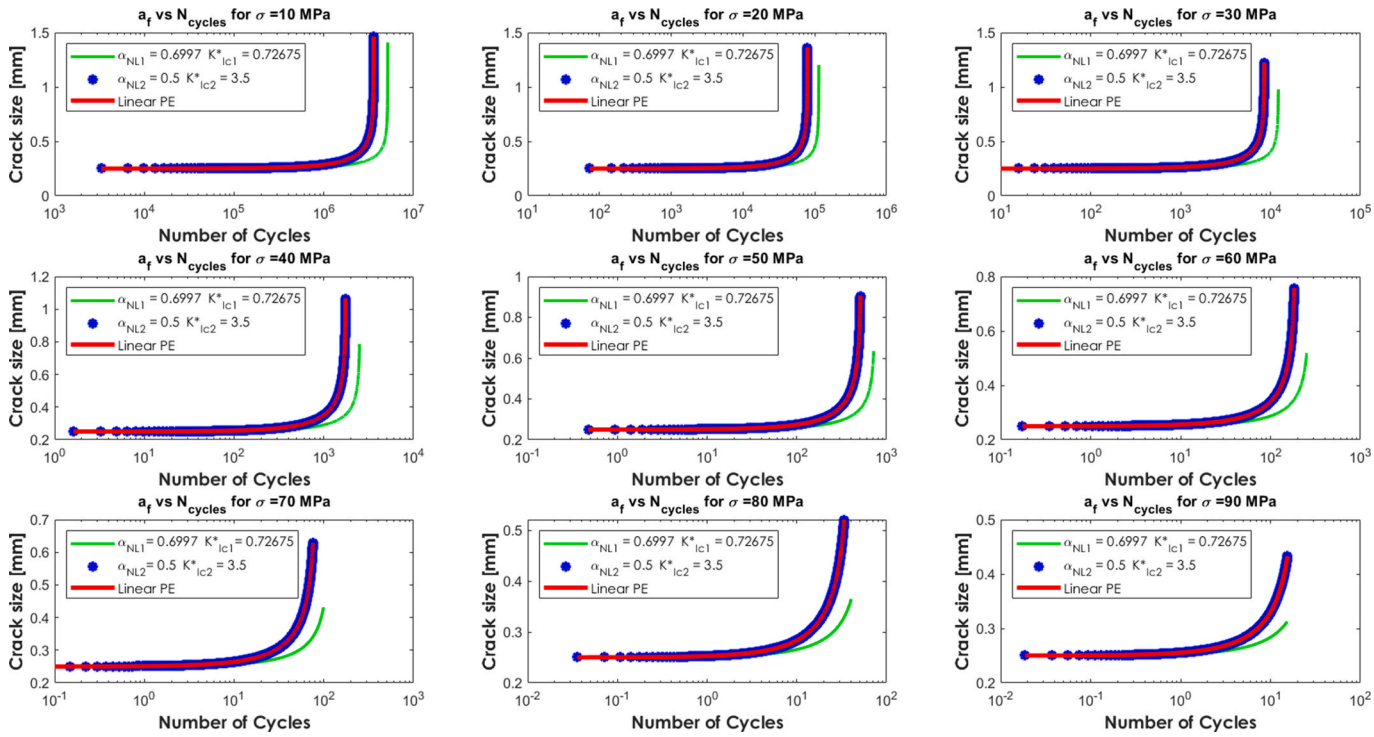

Fig. 4. Crack size growth for the different stress values for the non-linear GPE and linear PE approach, where the units of K^*_{IC} are $[MPa\, m^{\,\alpha}]$.

accuracy of MC analysis is determined by $(1/\sqrt{S})$, S being the number of samples. In particular, for the first analysis considering a uniform distribution, the parameter m_p was assumed to vary within the values $[m_{best\ fit} \pm 0.2 m_{best\ fit}]$, and the parameter C $(\mathrm{MPa}^{-m_p}\mathrm{m}^{m_p/2+1})$ between $[C_{best\ fit} \pm 0.2 C_{best\ fit}]$, meanwhile the value of the critical stress intensity factor K_{IC} $(\mathrm{MPa}\sqrt{\mathrm{m}})$ was introduced considering the results from the GA $K_{IC\ best\ fit}$. In the second analysis a normal distribution was considered, in which the parameter m_p was described by a mean of $m_{best\ fit}$ and a standard deviation of $m_{best\ fit} * 0.2$, while the parameter C was described by a mean of $C_{best\ fit}$ and a standard deviation of $C_{best\ fit} * 0.2$.

The range of the uniform distribution and the value of the standard deviation for the normal distribution were chosen to adequately capture

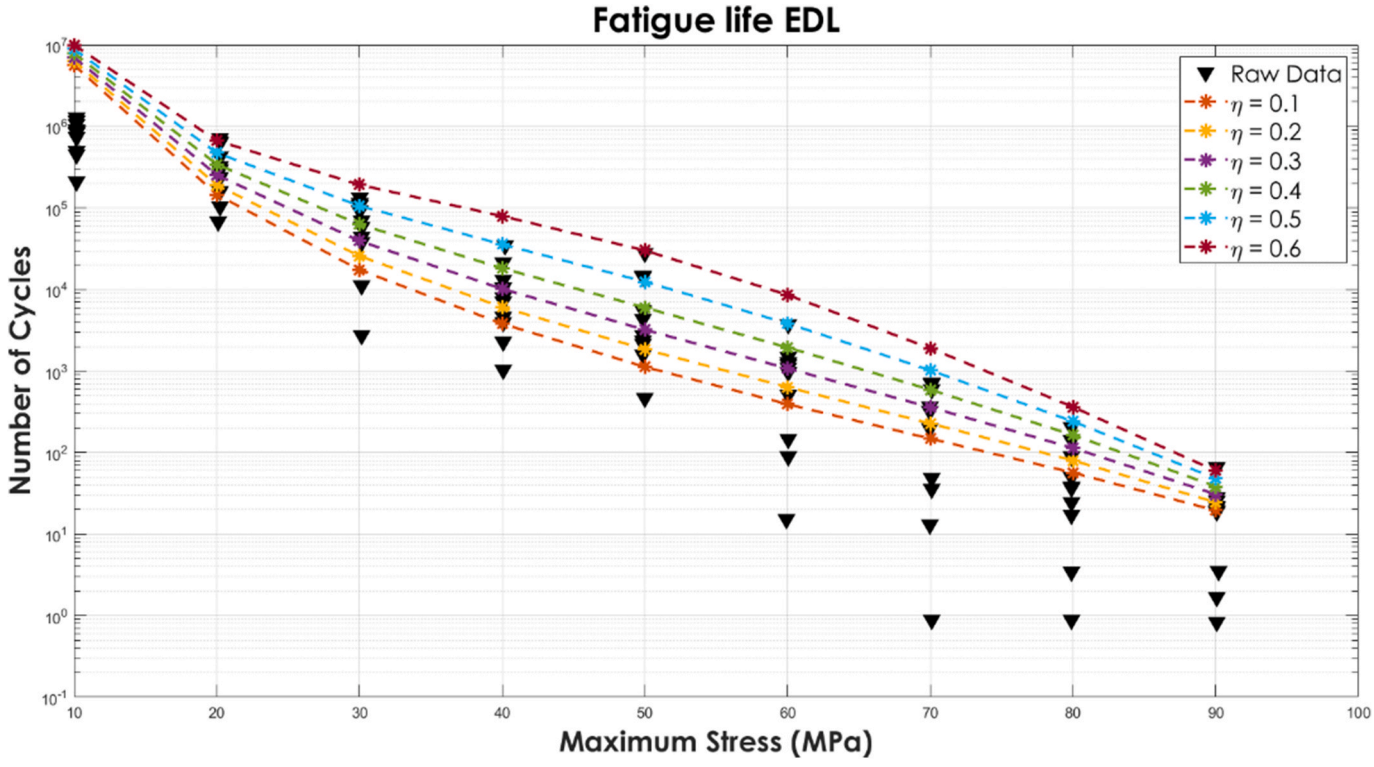

Fig. 5. Effect of the Healing function in the number of cycles for GPE approach.

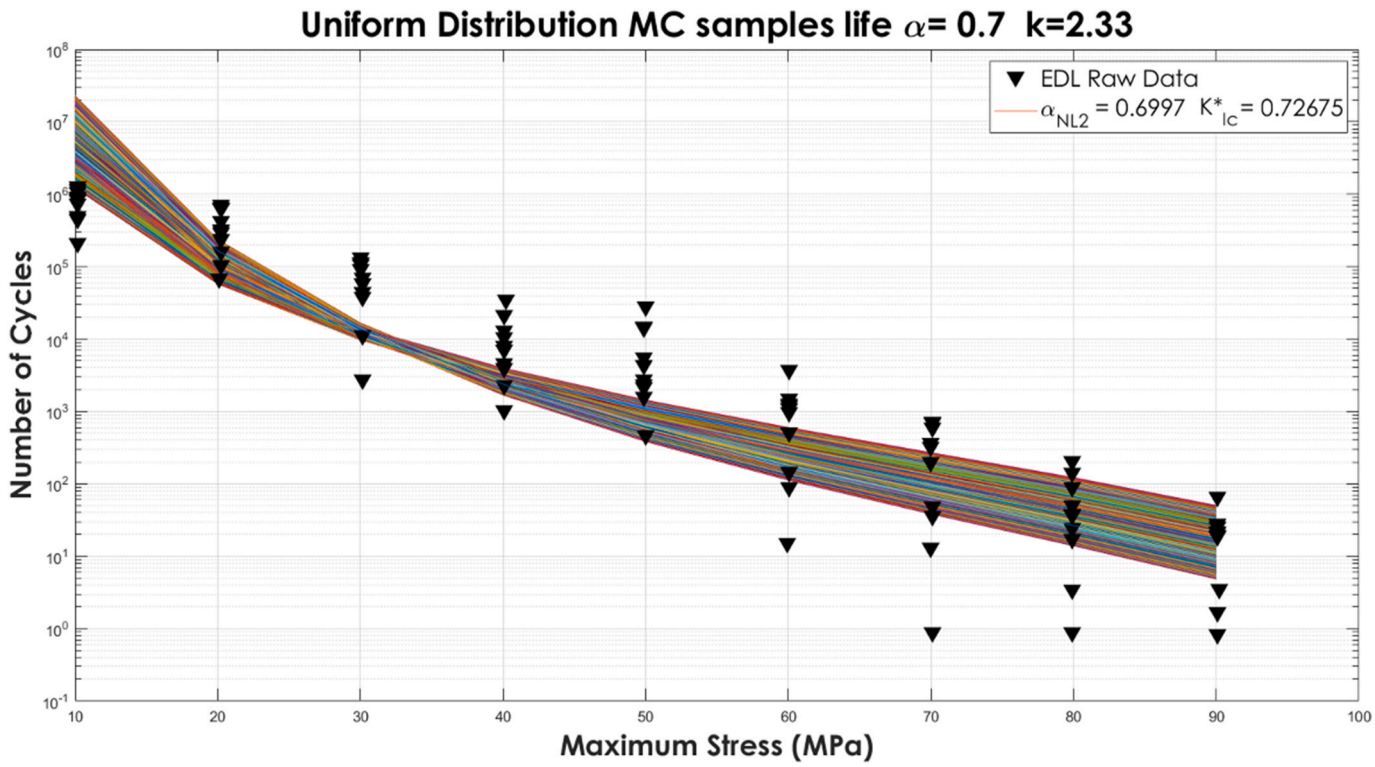

Fig. 6. Number of cycles obtained by Monte Carlo Analysis for the GPE approach with uniform distribution of m_p and C, where the units of K^*_{IC} are $[MPa\, m^{\alpha}]$.

the variability of the experimental data used in this study. This choice aligns with typical ranges observed in biological tissue measurements [49].

6. Results and discussion

6.1. Integration of the generalised Paris- Erdogan law for non-linear materials

Fig. 3 shows the curves obtained by the integration of the GEP law employing the results from the GA, here listed: $m_{best\ fit} = 5.5, K_{IC\ best\ fit} = 3.5\ MPa\sqrt{m}, C_{\ best\ fit} = 3 * 10^{-5} MPa^{-m_p} m^{m_p/2+1}$. The number of cycles in this graph and in the following figures is intended as the number of cycles after which failure occurs for the different stress levels. For comparison purposes, the traditional Paris-Erdogan (PE) law was integrated using results from the Genetic Algorithm (GA). Additionally, in the integration of the Generalised Paris-Erdogan (GPE) law, the parameter $\alpha = 0.5$, was also considered, as in this case the expression of the GPE law coincides with the traditional PE law. In Figs. 3 and 4 the results corresponding to the GPE law for $\alpha = 0.7$ are shown in green, while the blue lines represent curves obtained for $\alpha = 0.5$, and the red curves represent the values obtained by integrating the traditional PE law. The values obtained for the generalised critical SIF are also reported in the graph legend, being $K^*_{IC} = 0.73\ MPa\ m^{0.7}$, in case of $\alpha = 0.7$ and $K^*_{IC} = 3.5\ MPa\ m^{0.5}$ for $\alpha = 0.5$ that coincides with the value of the critical stress intensity factor obtained by the GA.

According to Fig. 3, it is evident that the number of cycles obtained for the GPE and linear PE law exhibits slight variations. Particularly, at lower stress levels, the variation is more pronounced compared to the values obtained at a stress level of 90 MPa. Furthermore, the values obtained for the lowest stress levels show an ineffective fit of the experimental data, leading to an overestimation in both cases.

From the integration of the GPE and linear PE law, it is possible to analyse the crack growth over the number of cycles for different max. Stress values. Fig. 4 displays the crack growth curves for all stress values in the experimental dataset. Observing the results, it stands out that the final crack size is smaller in the case of the GPE compared to the linear PE approach. In particular, the difference between the final crack size reached for the GPE and PE approaches is almost negligible at the stress value of 10 MPa. However, for higher stress values, the final crack size difference increases consistently as the stress value increases. Notably, the final crack size always remains smaller in the GPE non-linear approach compared to the linear PE one. Fig. 3 also reveals that, for the GPE approach, the number of cycles is higher than the linear PE approach, except for the values of 90 MPa, where both approaches yield nearly the same number of cycles.

6.2. Healing function influence on the number of cycles

Fig. 5 illustrates the impact of applying the healing function on the number of cycles obtained for the GPE approach with $\alpha = 0.7$. It is evident that the number of cycles increases whit the different stress levels up to the critical stress value σ_c, where the value of the healing function (HF) reaches its maximum (HF = η). The incorporation of the HF leads to a more accurate fit of the experimental data within the stress range of 20–80 MPa. Additionally, it is noteworthy that as the value of η increases, the number of cycles also increases proportionally. However, for stress values of 10 and 90 MPa, there is not a significant change in the number of cycles, as expected from the HF. It is important to highlight that no specific considerations can be drawn regarding the long-term effects of the healing application, given the absence of experimental in vivo data.

6.3. GPE for non-linear materials Monte Carlo analysis

The results of the MC analysis are presented in Fig. 6 for the GPE approach for the value of $\alpha = 0.7$ in case of a uniform distribution for the parameters m_p and C. In particular, the graph illustrates the substantial impact of introducing an uncertainty of 20% in only two parameters $C_{best\ fit}$ and $m_{best\ fit}$, which entails a significant change in the results. It is

Table 2
Statistics for the logarithm of the number of cycles (Log N) of first Monte Carlo simulation, C and m_p have uniform distributions.

Statistics for LogN									
Stress [MPa]	10	20	30	40	50	60	70	80	90
Mean	6.84	5.09	4.10	3.41	2.88	2.44	2.04	1.67	1.26
Std. dv.	6.70	4.60	3.20	2.66	2.34	2.02	1.71	1.38	1.00
Min	6.09	4.76	3.99	3.23	2.58	2.05	1.58	1.15	0.69
Max	7.36	5.38	4.22	3.60	3.16	2.78	2.43	2.09	1.70

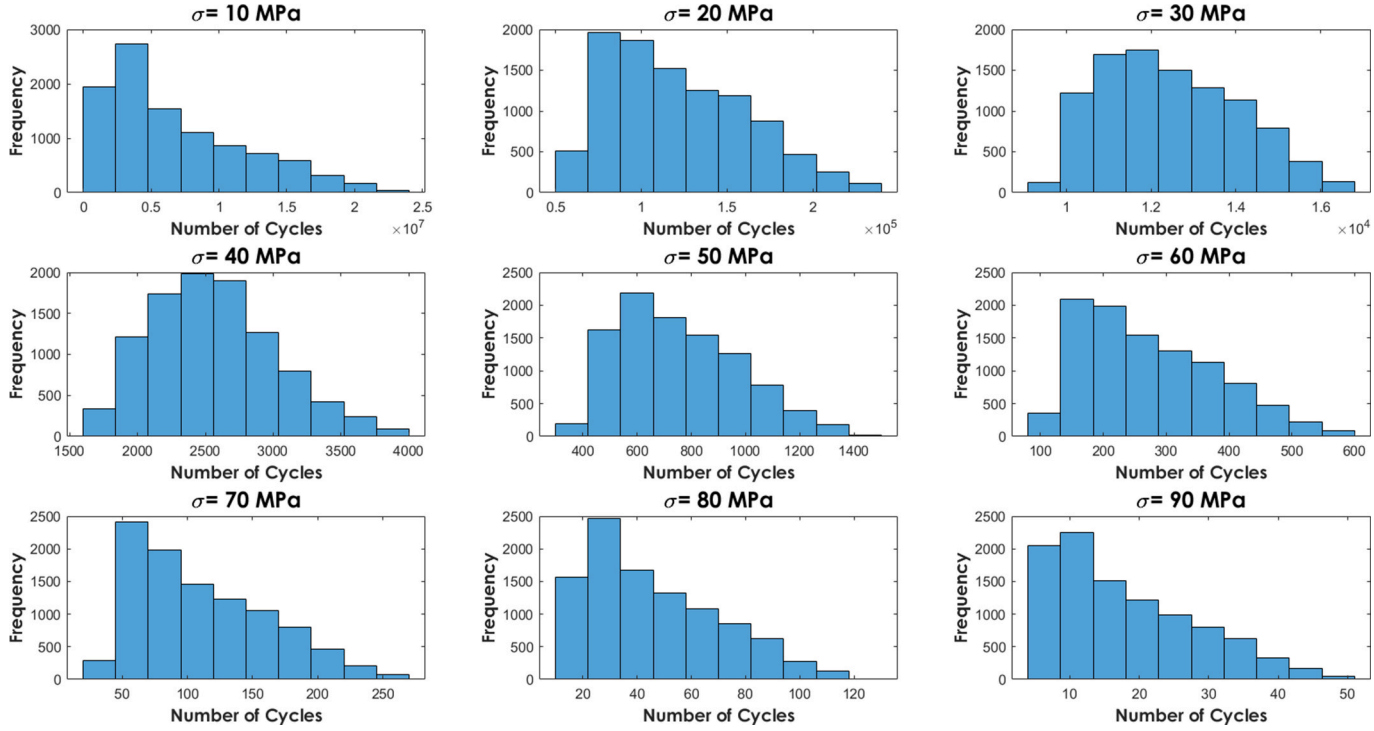

Fig. 7. Distributions of the number of cycles obtained with 10,000 samples run for the different stress values.

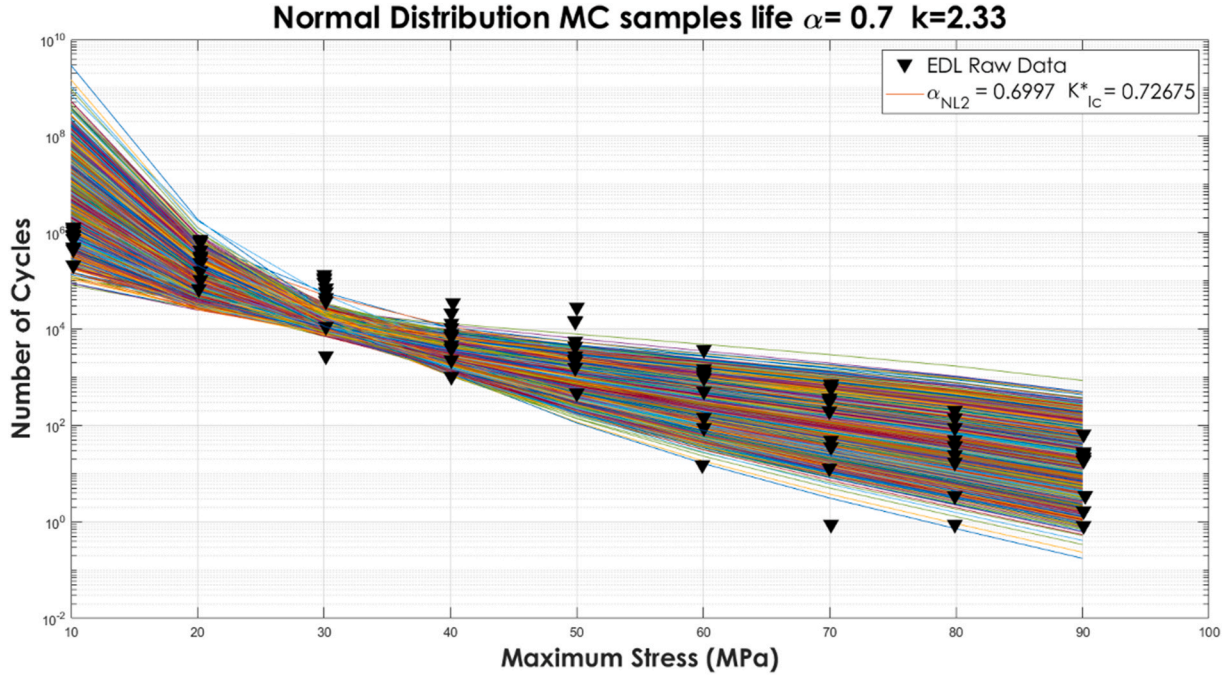

Fig. 8. Number of cycles obtained by Monte Carlo Analysis for the GPE approach with normal distribution of m_p and C, where the units of K^*_{IC} are $[MPa\, m^{\alpha}]$.

Table 3
Statistics for the logarithm of the number of cycles (Log N) for the second Monte Carlo simulation.

Statistics for LogN									
Stress [MPa]	10	20	30	40	50	60	70	80	90
Mean	7.09	5.14	4.12	3.44	2.94	2.52	2.16	1.81	1.42
Std. dv.	7.42	4.96	3.52	2.99	2.71	2.43	2.17	1.88	1.55
Min	4.82	4.35	3.83	2.96	2.12	1.42	0.83	0.29	0.26
Max	8.82	6.11	4.72	4.23	4.03	3.84	3.63	3.40	3.11

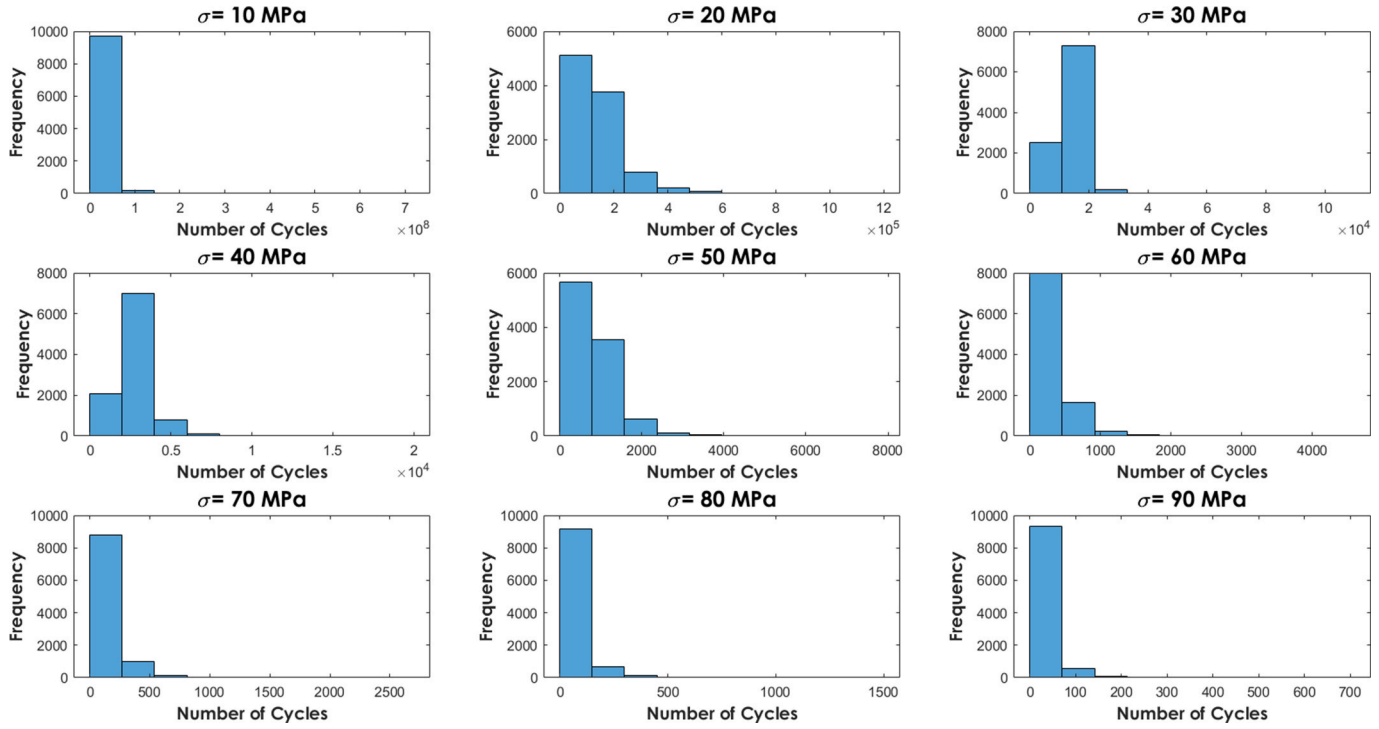

Fig. 9. Distributions of the number of cycles obtained with 10,000 samples runs for the different stress values.

noticeable that the bounds amplitude is wider for lower and higher stress levels. Meanwhile, in correspondence to the stress values of 30–40 MPa, the bounds exhibit the narrowest amplitude. It has been observed that the tightest bounds consistently occur at 30–40 MPa for different values of α. Although most of the experimental points are within the bounds, there are some outliers. Specifically, those corresponding to stress values within the range of 20–50 MPa, where the interval for the number of cycles becomes narrower. The statistics for the first Monte Carlo simulation are shown in Table 2, where LogN is the logarithm of the number of cycles for the different stress values.

Fig. 7 displays the diverse distributions of the number of cycles obtained for various stress values. For almost all stress values, the observed number of cycles exhibits similar distributions. However, a quasi-normal distribution shape is observed only in the case of stress values at 30 and 40 MPa, where the bounds are narrower.

Fig. 8 displays the number of cycles obtained for the second case Monte Carlo analysis, where the values of m_p and C follow a normal distribution. In this scenario, introducing a standard deviation of 20% of the mean value results in a greater dispersion of the obtained cycles. Notably, almost all experimental data are covered by the Monte Carlo simulation results in this analysis. It is worth mentioning that, similarly to the first analysis, the narrowest section of the bounds corresponds to stress levels of 30–40 MPa. Table 3 presents the statistics for the second Monte Carlo simulation.

The distributions for the number of cycles at each stress level are depicted in Fig. 9. In contrast to the previous distributions, in this case, with the same quantity of groups (10 for the histogram), it is evident that almost all values are concentrated in two or three classes out of 10. The uniform distribution results in a broader range of cycle values compared to the previous case. However, it is noteworthy that values with high frequency coincide with those obtained under the uniform distribution.

7. Conclusions

The proposed generalisation of the Paris-Erdogan law for non-linear materials suggests that incorporating non-linearities into the Paris-Erdogan law designed for linear elastic materials does not yield significant improvements in terms of fitting experimental data, at least based on the examined case study. This leads to the consideration that, even though the Paris-Erdogan law was originally formulated for linear elastic materials, it may also find applicability for non-linear materials with a constitutive law analogous to that of the biological material constituting tendons. However, further investigation on this aspect is necessary, ideally with additional experimental data from specimens of various materials characterised by a non-linear polynomial constitutive law.

In this study, the mechanical parameters C and m_p for the PE law have been estimated in the case of tendons. Further studies are necessary to effectively validate these values. The introduction of the HF allows to observe an increase of the number of cycles for each stress value. This was expected, as self-healing is present in natural structures as a consequence of evolution and allows to repair the micro damages

induced by physiological loads. However, additional investigations are needed to assess the hypothesis of the healing function's dependence on the stress levels as the most suitable representation for the healing process. The high variability among the samples, and their related mechanical and fatigue properties, allows to obtain reasonable bounds for a uniform distribution for the parameters for the GPE approach. In particular, it was observed that the Generalised Paris-Erdogan (GPE) approach exhibits high sensitivity to changes in input parameters under high and low stress conditions compared to medium stresses. This underscores the necessity for a comprehensive understanding of the model's behaviour under different stress conditions, emphasising the need for further research to refine and validate the proposed approach in various scenarios.

CRediT authorship contribution statement

Mariana Rodriguez Reinoso: Writing – original draft, Validation, Software, Investigation, Formal analysis. **Paola Antonaci:** Writing – review & editing, Supervision, Data curation, Conceptualization. **Nicola M. Pugno:** Writing – review & editing, Validation, Supervision, Formal analysis, Conceptualization. **Cecilia Surace:** Writing – review & editing, Supervision, Methodology, Conceptualization.

Declaration of competing interest

The authors declare that they have no known competing financial interests or personal relationships that could have appeared to influence the work reported in this paper. The author is an Editorial Board Member/Editor-in-Chief/Associate Editor/Guest Editor for [Journal name] and was not involved in the editorial review or the decision to publish this article. The authors declare the following financial interests/personal relationships which may be considered as potential competing interests.

Data availability

The authors do not have permission to share data.

Acknowledgments

The authors express their gratitude to Dr. Rinto Roy and Mr. Vito Burgio for their valuable suggestions and support.

References

[1] F. Fang, S.P. Lake, Modelling approaches for evaluating multiscale tendon mechanics, Interface Focus 6 (1) (Feb. 06, 2016), https://doi.org/10.1098/rsfs.2015.0044. Royal Society of London.
[2] R.F. Ker, Dynamic Tensile Properties of the Plantaris Tendon of Sheep (Ovis Aries), 1981.
[3] H.R.C. Screen, Hierarchical approaches to understanding tendon mechanics, J. Biomech. Sci. Eng. 4 (4) (2009) 481–499, https://doi.org/10.1299/jbse.4.481.
[4] A.A. Biewener, Tendons and ligaments: structure, mechanical behavior and biological function, Collagen (2008) 269–284.
[5] G.A. Lichtwark, A.M. Wilson, In vivo mechanical properties of the human Achilles tendon during one-legged hopping, J. Exp. Biol. 208 (24) (Dec. 2005) 4715–4725, https://doi.org/10.1242/jeb.01950.
[6] J.H.C. Wang, Mechanobiology of tendon, J. Biomech. 39 (9) (2006) 1563–1582, https://doi.org/10.1016/j.jbiomech.2005.05.011.
[7] J.H. Shepherd, H.R.C. Screen, Fatigue loading of tendon, Int. J. Exp. Pathol. 94 (4) (Aug. 2013) 260–270, https://doi.org/10.1111/iep.12037.
[8] U. Giuseppe Longo, M. Ronga, N. Maffulli, Achilles Tendinopathy, 2009 [Online]. Available: www.sportsmedarthro.com.
[9] N. Maffulli, U.G. Longo, A. Kadakia, F. Spiezia, Achilles tendinopathy, Foot Ankle Surg. 26 (3) (Apr. 01, 2020) 240–249, https://doi.org/10.1016/j.fas.2019.03.009. Elsevier Ltd.
[10] M.I. Boyer, C.A. Goldfarb, R.H. Gelberman, Recent progress in flexor tendon healing: the modulation of tendon healing with rehabilitation variables, J. Hand Ther. 18 (2) (2005) 80–85, https://doi.org/10.1197/j.jht.2005.01.009.
[11] J.D. Urschel, P.G. Scottand, H.T.G. Williams, The effect of mechanical stress on soft and hard tissue repair; a review, Br. J. Plast. Surg. 41 (1988) 182–186.
[12] C. Martin, W. Sun, Fatigue damage of collagenous tissues: experiment, modeling and simulation studies, J. Long Term Eff. Med. Implants 25 (2015) 55–73.
[13] X.T. Wang, R.F. Ker, Fatigue rupture of wallaby tail tendons, J. Exp. Biol. 198 (1995) 847–852.
[14] R.F. Ker, X.T. Wang, A.V.L. Pike, Fatigue quality of mammalian tendons, J. Exp. Biol. 203 (2000) 1317–1327.
[15] K. Pedaprolu, S.E. Szczesny, A novel, open-source, low-cost bioreactor for load-controlled cyclic loading of tendon explants, J. Biomech. Eng. 144 (8) (Aug. 2022), https://doi.org/10.1115/1.4053795.
[16] D.T. Fung, et al., Subrupture tendon fatigue damage, J. Orthop. Res. 27 (2) (Feb. 2009) 264–273, https://doi.org/10.1002/jor.20722.
[17] L.J. Soslowsky, et al., Overuse activity injures the supraspinatus tendon in an animal model: a histologic and biomechanical study, J. Shoulder Elbow Surg. 9 (2) (2000) 79–84, https://doi.org/10.1067/mse.2000.101962.
[18] A. Scott, J.L. Cook, D.A. Hart, D.C. Walker, V. Duronio, K.M. Khan, Tenocyte responses to mechanical loading in vivo, Arthritis Rheum. 56 (3) (Mar. 2007) 871–881, https://doi.org/10.1002/art.22446.
[19] D.T. Fung, et al., Early response to tendon fatigue damage accumulation in a novel in vivo model, J. Biomech. 43 (2) (Jan. 2010) 274–279, https://doi.org/10.1016/j.jbiomech.2009.08.039.
[20] N. Andarawis-Puri, E.L. Flatow, Tendon fatigue in response to mechanical loading, J. Musculoskelet. Neuronal Interact. 11 (2) (2011) 106–114.
[21] J.B. Sereysky, N. Andarawis-Puri, K.J. Jepsen, E.L. Flatow, Structural and mechanical effects of in vivo fatigue damage induction on murine tendon, J. Orthop. Res. 30 (6) (Jun. 2012) 965–972, https://doi.org/10.1002/jor.22012.
[22] H. Schechtman, D.L. Bader, In vitro fatigue of human tendons, J. Biomech. 30 (8) (1997) 829–835.
[23] T.A.L. Wren, D.P. Lindsey, G.S. Beaupré, D.R. Carter, Effects of creep and cyclic loading on the mechanical properties and failure of human Achilles tendons, Ann. Biomed. Eng. 31 (6) (2003) 710–717, https://doi.org/10.1114/1.1569267.
[24] C.R. Firminger, W.B. Edwards, Effects of cyclic loading on the mechanical properties and failure of human patellar tendon, J. Biomech. 120 (May 2021), https://doi.org/10.1016/j.jbiomech.2021.110345.
[25] B.R. Freedman, J.J. Sarver, M.R. Buckley, P.B. Voleti, L.J. Soslowsky, Biomechanical and structural response of healing Achilles tendon to fatigue loading following acute injury, J. Biomech. 47 (9) (Jun. 2014) 2028–2034, https://doi.org/10.1016/j.jbiomech.2013.10.054.
[26] T.W. Herod, N.C. Chambers, S.P. Veres, Collagen fibrils in functionally distinct tendons have differing structural responses to tendon rupture and fatigue loading, Acta Biomater. 42 (Sep. 2016) 296–307, https://doi.org/10.1016/j.actbio.2016.06.017.
[27] J. Gregory, A.L. Hazel, T. Shearer, A microstructural model of tendon failure, J. Mech. Behav. Biomed. Mater. 122 (Oct) (2021), https://doi.org/10.1016/j.jmbbm.2021.104665.
[28] K. Linka, M. Hillgärtner, M. Itskov, Fatigue of soft fibrous tissues: multi-scale mechanics and constitutive modeling, Acta Biomater. 71 (Apr. 2018) 398–410, https://doi.org/10.1016/j.actbio.2018.03.010.
[29] C. Martin, W. Sun, Simulation of long-term fatigue damage in bioprosthetic heart valves: effects of leaflet and stent elastic properties, Biomech. Model. Mechanobiol. 13 (4) (2014) 759–770, https://doi.org/10.1007/s10237-013-0532-x.
[30] F. Bosia, M. Merlino, N.M. Pugno, Fatigue of self-healing hierarchical soft nanomaterials: the case study of the tendon in sportsmen, J. Mater. Res. 30 (1) (Sep. 2014) 2–9, https://doi.org/10.1557/jmr.2014.335.
[31] S.M. Adeeb, M.L. Zec, G.M. Thornton, C.B. Frank, N.G. Shrive, A novel application of the principles of Linear Elastic Fracture Mechanics (LEFM) to the fatigue behavior of tendon tissue, J. Biomech. Eng. 126 (5) (Oct. 2004) 641–650, https://doi.org/10.1115/1.1800556.
[32] S.H. Hosseini Nasab, et al., Uncertainty in muscle–tendon parameters can greatly influence the accuracy of knee contact force estimates of musculoskeletal models, Front. Bioeng. Biotechnol. 10 (Jun) (2022), https://doi.org/10.3389/fbioe.2022.808027.
[33] D. Balzani, T. Schmidt, M. Ortiz, Method for the quantification of rupture probability in soft collagenous tissues, Int. J. Numer. Method Biomed. Eng. 33 (1) (Jan. 2017), https://doi.org/10.1002/cnm.2781.
[34] J. Haughton, S.L. Cotter, W.J. Parnell, T. Shearer, Bayesian inference on a microstructural, hyperelastic model of tendon deformation, J. R. Soc. Interface 19 (190) (2022), https://doi.org/10.1098/rsif.2022.0031.
[35] K. Worden, G. Manson, Prognosis under Uncertainty-An Idealised Computational Case Study, 2008.
[36] C. Surace, K. Worden, Extended analysis of a damage prognosis approach based on interval arithmetic, Strain 47 (6) (Dec. 2011) 544–554, https://doi.org/10.1111/j.1475-1305.2011.00815.x.
[37] A. Carpinteri, N. Pugno, Cracks and re-entrant corners in functionally graded materials, Eng. Fract. Mech. 73 (10) (Jul. 2006) 1279–1291, https://doi.org/10.1016/j.engfracmech.2006.01.008.
[38] N. Pugno, A. Carpinteri, M. Ippolito, A. Mattoni, L. Colombo, Atomistic fracture: QFM vs. MD, Eng. Fract. Mech. 75 (7) (May 2008) 1794–1803, https://doi.org/10.1016/j.engfracmech.2007.01.028.
[39] G.A. Von Forell, P.S. Hyoung, A.E. Bowden, Failure modes and fracture toughness in partially torn ligaments and tendons, J. Mech. Behav. Biomed. Mater. 35 (2014) 77–84, https://doi.org/10.1016/j.jmbbm.2014.03.020.
[40] D. Taylor, N. O'Mara, E. Ryan, M. Takaza, C. Simms, The fracture toughness of soft tissues, J. Mech. Behav. Biomed. Mater. 6 (Feb. 2012) 139–147, https://doi.org/10.1016/j.jmbbm.2011.09.018.
[41] J.R. Rice, G.F. Rosengren, Plane Strain Deformation Near a Crack Tip in a Power-Law Hardening Material, Pergamon Press, 1968.

[42] B.R. Howard, Control of variability, ILAR J. 43 (4) (2002) 194–201 [Online]. Available: https://academic.oup.com/ilarjournal/article/43/4/194/981669.
[43] J.F. Weber, A.M.R. Agur, A.Y. Fattah, K.D. Gordon, M.L. Oliver, Tensile mechanical properties of human forearm tendons, J. Hand Surg.: European Volume 40 (7) (Sep. 2015) 711–719, https://doi.org/10.1177/1753193415584715.
[44] [Online]. Available: www.elsevier.com/locate/flowmeasinst C.E. Papadopoulos, H. Yeung, Uncertainty estimation and Monte Carlo simulation method, , 2001.
[45] M. Shan, L. Zhao, J. Ye, A novel micromechanics-model-based probabilistic analysis method for the elastic properties of unidirectional CFRP composites, Materials 15 (15) (Aug. 2022), https://doi.org/10.3390/ma15155090.
[46] E. Van Houten, G. Geymonat, F. Krasucki, B. Wattrisse, General guidelines for the performance of viscoelastic property identification in elastography: a Monte-Carlo analysis from a closed-form solution, Int. J. Numer. Method Biomed. Eng. 39 (8) (Aug. 2023), https://doi.org/10.1002/cnm.3741.
[47] D.C. Ackland, Y.C. Lin, M.G. Pandy, Sensitivity of model predictions of muscle function to changes in moment arms and muscle-tendon properties: a Monte-Carlo analysis, J. Biomech. 45 (8) (May 2012) 1463–1471, https://doi.org/10.1016/j.jbiomech.2012.02.023.